nature medicine

Rejuvenation of the muscle stem cell population restores strength to injured aged muscles

Benjamin D Cosgrove[1], Penney M Gilbert[1,2], Ermelinda Porpiglia[1], Foteini Mourkioti[1], Steven P Lee[1], Stephane Y Corbel[1], Michael E Llewellyn[3], Scott L Delp[3,4] & Helen M Blau[1]

The elderly often suffer from progressive muscle weakness and regenerative failure. We demonstrate that muscle regeneration is impaired with aging owing in part to a cell-autonomous functional decline in skeletal muscle stem cells (MuSCs). Two-thirds of MuSCs from aged mice are intrinsically defective relative to MuSCs from young mice, with reduced capacity to repair myofibers and repopulate the stem cell reservoir *in vivo* following transplantation. This deficiency is correlated with a higher incidence of cells that express senescence markers and is due to elevated activity of the p38α and p38β mitogen-activated kinase pathway. We show that these limitations cannot be overcome by transplantation into the microenvironment of young recipient muscles. In contrast, subjecting the MuSC population from aged mice to transient inhibition of p38α and p38β in conjunction with culture on soft hydrogel substrates rapidly expands the residual functional MuSC population from aged mice, rejuvenating its potential for regeneration and serial transplantation as well as strengthening of damaged muscles of aged mice. These findings reveal a synergy between biophysical and biochemical cues that provides a paradigm for a localized autologous muscle stem cell therapy for the elderly.

During aging, skeletal muscle strength progressively declines (sarcopenia), leading to reduced mobility, muscle function and quality of life[1,2]. A number of pharmacologic strategies to treat muscle wasting have been proposed that are directed at reversing myofiber atrophy or promoting myofiber hypertrophy and are largely designed to target mitochondrial, catabolic and anabolic mechanisms in the context of cachexia or sarcopenia[3–6]. Despite these major advances, no pharmacologic therapies are currently in clinical use that ameliorate or reverse the decline in muscle strength in the elderly[7,8], which constitutes a costly and ever-increasing healthcare concern[9].

An alternative or synergistic strategy for increasing muscle strength enlists the regenerative capacity of muscle stem cells (MuSCs; also known as satellite cells[10–12]) that reside on muscle fibers and are dedicated to their repair. As MuSC numbers remain relatively constant during aging in mice and humans until late in life, a reduced stem cell abundance does not fully account for the impaired regeneration observed during aging[13]. Instead, several reports attribute loss of muscle regenerative capacity to changes in the aged systemic and local microenvironments, not to the stem cells themselves[2,14–18]. For example, systemic factors from young mice ameliorate muscle regeneration in aged mice following heterochronic parabiosis[15,17]. In addition, targeting microenvironmental factors characteristic of aged muscle tissues, such as signaling via the Wnt, Notch, transforming growth factor-β and fibroblast growth factor pathways, enhances regeneration[15,16,18,19].

Here we show that the MuSC population from aged mice is inherently defective in its essential functions of regenerating damaged myofibers and repopulating the stem cell reserve. We demonstrate that the reduced function of MuSCs from aged mice can be overcome in culture by the combined effects of a small-molecule inhibitor of p38α and p38β (here called p38α/β) mitogen-activated protein kinase (MAPK) and a porous hydrogel substrate with biophysical properties matching the soft elasticity of muscle tissue. The synergistic combination of these biochemical and biophysical cues stimulates the rapid expansion of functional stem cells within the progeny of MuSCs from aged mice to generate a stem cell population with rejuvenated function capable of restoring strength to injured muscles from aged mice.

RESULTS

MuSCs from aged mice have autonomous regeneration defects

Transplantation of purified muscle stem cells in conjunction with a sensitive imaging assay of engraftment, a measure of regeneration, first revealed that MuSCs from aged mice (24 months old) have intrinsic defects and are two-thirds less effective than MuSCs from young mice (2 months old) in regenerating muscle (**Fig. 1**). Recent studies have described methods to prospectively isolate MuSCs from mice to high purity by FACS[11,20–25]. Thus, we isolated and enriched MuSCs from young and aged mice by FACS for $CD45^-CD31^-CD11b^-Sca1^-CD34^+$integrin α_7^+ cells to ≥95% purity, as previously described[11]

[1]Baxter Laboratory for Stem Cell Biology, Department of Microbiology and Immunology, and Institute for Stem Cell Biology and Regenerative Medicine, Stanford University School of Medicine, Stanford, California, USA. [2]Institute of Biomaterials and Biomedical Engineering and Donnelly Centre for Cellular and Biomolecular Research, University of Toronto, Toronto, Ontario, Canada. [3]Department of Bioengineering, Stanford University School of Medicine, Stanford, California, USA. [4]Department of Mechanical Engineering, Stanford University School of Medicine, Stanford, California, USA. Correspondence should be addressed to H.M.B. (hblau@stanford.edu) or P.M.G. (penney.gilbert@utoronto.ca).

Received 2 March 2013; accepted 11 January 2014; published online 16 February 2014; doi:10.1038/nm.3464

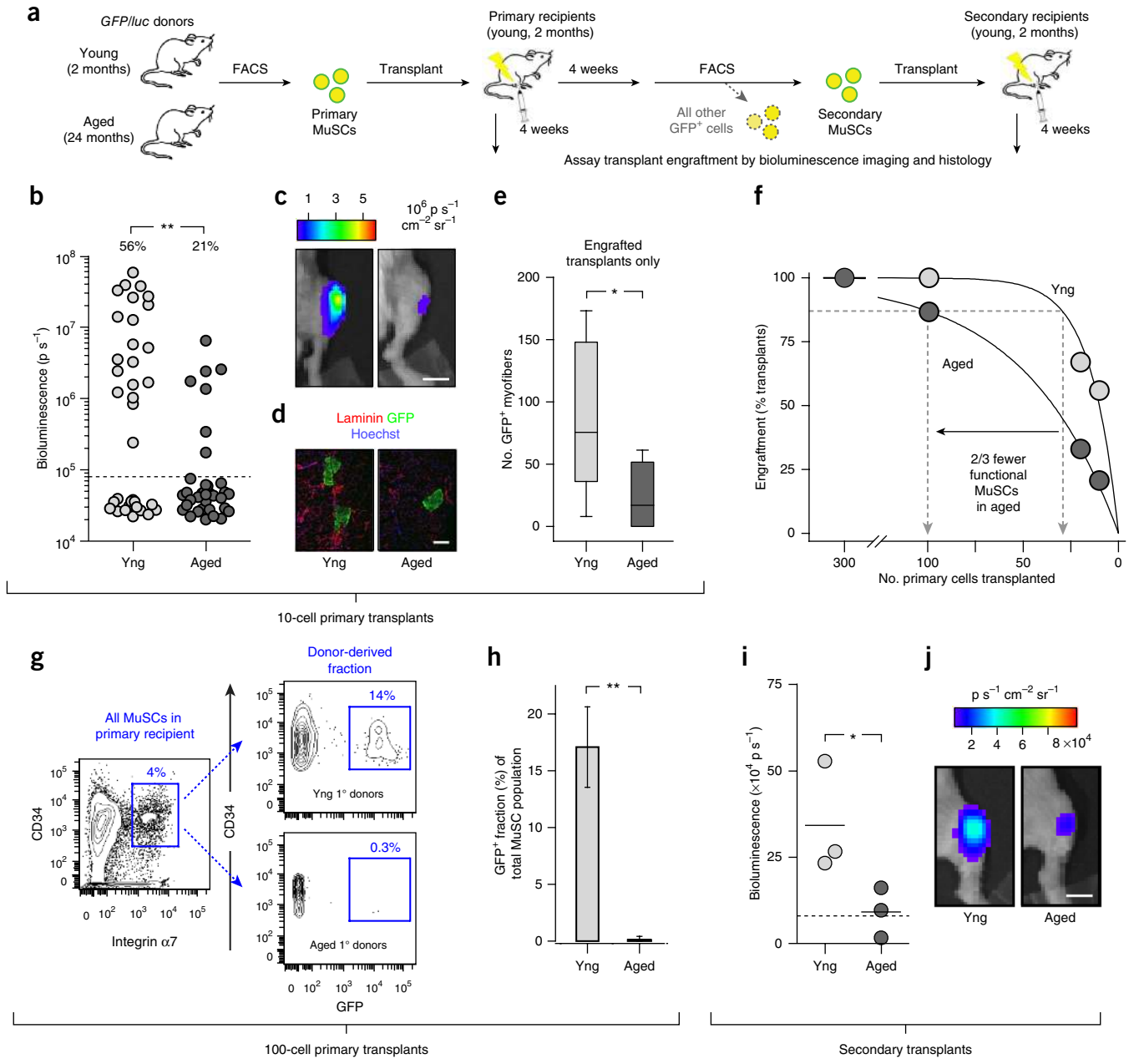

Figure 1 MuSCs from aged mice have diminished regenerative and self-renewal capacity, revealing an inherent stem cell defect. (**a**) MuSC intramuscular transplantation scheme. (**b**–**e**) BLI and immunohistology of ten-cell primary transplants from young (Yng) or aged *GFP/luc* MuSC donors. (**b**) BLI signals from $n = 34$ recipients from three experiments. p, photons. Engraftment threshold (dashed line) corresponding to histological detection of ≥1 donor-derived (GFP$^+$) myofibers in **b** and **i**. (**c**) Representative BLI images. Scale bar, 5 mm. (**d**) Representative immunohistological images. Scale bar, 500 µm. (**e**) GFP$^+$ myofibers per recipient tibialis anterior muscle ($n = 6$ or 7 recipients from three experiments) in engrafted samples. Graph shows median central line, 50% confidence interval box and 95% confidence interval whiskers. (**f**) Limiting-dilution analysis relating primary MuSCs transplanted with percentage engraftment from $n = 5$–34 transplants per condition. (**g**,**h**) Flow cytometric analysis of GFP$^+$ fraction of all CD34$^+$integrin α_7^+ MuSCs in primary recipients ($n = 3$, mean ± s.e.m.) transplanted with 100 primary (1°) MuSCs from young or aged mice. (**i**,**j**) Analysis of $n = 3$ secondary recipients transplanted with reisolated GFP$^+$CD34$^+$integrin α_7^+ cells from $n = 10$ recipients of 700 primary MuSCs from young or aged mice. (**i**) Secondary recipient BLI scatter plot (mean line). (**j**) Representative BLI images. Scale bar, 5 mm. $^*P < 0.05$ or $^{**}P < 0.01$ by Fisher's exact test (**b**), Mann-Whitney *U*-test (**e**), Student's *t*-test (**h**) and paired *t*-test (**i**).

(**Supplementary Fig. 1a**). We employed limiting-dilution analysis, a standard assay in the hematopoiesis field[26], to quantify and compare the frequency of cells with stem cell function within heterogeneous prospectively isolated populations. We injected different numbers (10, 20, 100 or 300 cells) of freshly isolated MuSCs from young or aged donor mice intramuscularly into irradiated hindlimb muscles of young nonobese diabetic–severe combined immunodeficiency (NOD-SCID) mice (**Fig. 1a**–**f**). Donor MuSCs were isolated from transgenic C57BL/6/FVB mice expressing GFP and the enzyme firefly luciferase (*GFP/luc* mice). We monitored transplant engraftment *in vivo* by bioluminescence imaging (BLI) and confirmed the results by standard retrospective GFP immunohistochemistry[11]. BLI is well suited to an

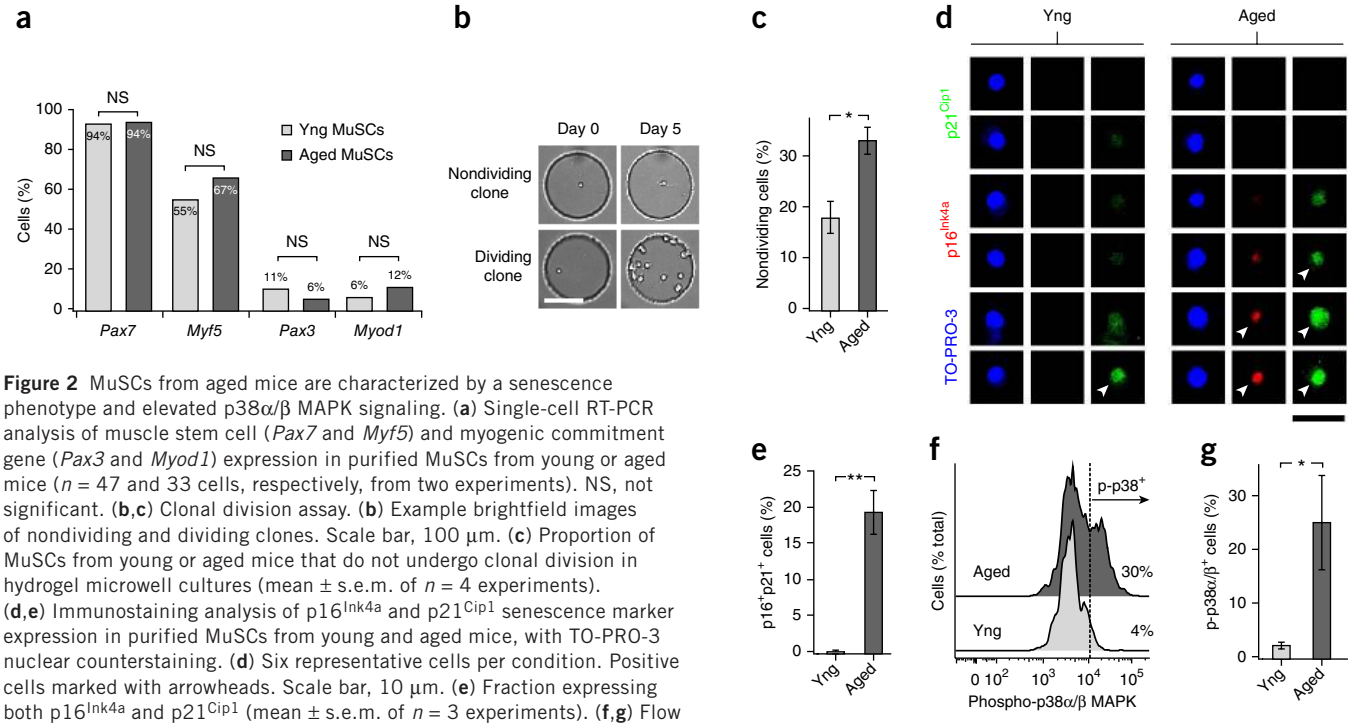

Figure 2 MuSCs from aged mice are characterized by a senescence phenotype and elevated p38α/β MAPK signaling. (**a**) Single-cell RT-PCR analysis of muscle stem cell (*Pax7* and *Myf5*) and myogenic commitment gene (*Pax3* and *Myod1*) expression in purified MuSCs from young or aged mice ($n = 47$ and 33 cells, respectively, from two experiments). NS, not significant. (**b**,**c**) Clonal division assay. (**b**) Example brightfield images of nondividing and dividing clones. Scale bar, 100 µm. (**c**) Proportion of MuSCs from young or aged mice that do not undergo clonal division in hydrogel microwell cultures (mean ± s.e.m. of $n = 4$ experiments). (**d**,**e**) Immunostaining analysis of $p16^{Ink4a}$ and $p21^{Cip1}$ senescence marker expression in purified MuSCs from young and aged mice, with TO-PRO-3 nuclear counterstaining. (**d**) Six representative cells per condition. Positive cells marked with arrowheads. Scale bar, 10 µm. (**e**) Fraction expressing both $p16^{Ink4a}$ and $p21^{Cip1}$ (mean ± s.e.m. of $n = 3$ experiments). (**f**,**g**) Flow cytometric analysis of phospho-p38α/β MAPK in purified MuSCs from young or aged mice. (**f**) Representative histograms from $n = 3$ experiments. (**g**) Bar plot of phospho-p38α/β$^+$ cell frequency (mean ± s.e.m., $n = 3$). $^*P < 0.05$ or $^{**}P < 0.01$ by Fisher's exact test (**a**) and Student's *t*-test (**c**, **e** and **g**).

analysis of low numbers of transplanted luciferase-expressing MuSCs, as it can sensitively capture the engraftment and dynamic expansion of an initially undetectable small population of cells (**Supplementary Fig. 1b**). We observed that BLI levels correlate well with immunohistochemical measures of GFP$^+$ MuSC fusion to myofibers, as we have reported previously[11] (**Supplementary Fig. 1c**).

We observed no difference in engraftment frequency upon transplantation of 100 or more cells (**Fig. 1f**), which is in agreement with previous studies[18]. However, when we delivered as few as ten cells, a defect was apparent, as we found that MuSC transplants from aged mice engrafted at a markedly lower frequency than MuSC transplants from young mice. Thus, the intrinsic defect in MuSCs from aged mice was masked when higher numbers were transplanted. Both the fraction of transplants that engrafted and the number of GFP$^+$ myofibers observed in engrafted recipients were lower (**Fig. 1b–f**). These differences were not due to sex, as similar results were observed with donor MuSCs from male and female mice (**Supplementary Fig. 1d**). Analysis of the transplant results using a stem cell limiting-dilution model[26] revealed that MuSCs from aged mice have a two-thirds lower incidence of functional stem cells than MuSCs from young mice (**Fig. 1f** and **Supplementary Fig. 1e**). Thus, this sensitive and quantitative assay revealed that, even in the microenvironment of young muscles, the proportion of MuSCs isolated from aged mice that displayed repair function was much lower than that of MuSCs isolated from young mice, owing to an autonomous cell-intrinsic defect.

MuSCs from aged mice are impaired in serial transplantation

The most exacting measure of long-term MuSC potential is serial transplantation, the ability of MuSCs to regenerate tissues in successive recipients[27,28]. We established a serial transplantation assay to compare long-term function of MuSCs from young and aged *GFP/luc* transgenic mice (**Fig. 1a**). First, we evaluated stem cell repopulation in primary recipients by flow cytometric detection of donor-derived (GFP$^+$) MuSCs as a fraction of the total recipient MuSC (CD34$^+$integrin α_7^+) population 1 month after transplantation (**Fig. 1g**). To compare stem cell repopulation potential between MuSCs isolated from young and aged mice, we performed transplants with a range of cell numbers (100, 200 and 700 cells), enabling a comparative limiting-dilution analysis. MuSCs from aged mice gave rise to a substantially smaller fraction of the total MuSC population in primary recipients than did MuSCs isolated from young mice (**Fig. 1h** and **Supplementary Fig. 2a**). These results provide further evidence for a cell-autonomous stem cell self-renewal defect in MuSCs from aged mice.

We immediately transplanted the entire population of GFP$^+$ MuSCs isolated by FACS from primary recipient muscles into secondary recipient muscles. We compared the GFP$^+$ fraction of the CD34$^+$integrin α_7^+ MuSC population (**Supplementary Fig. 2b**,**c**) and used a relatively high number of MuSCs (700 cells) in the primary transplants to ensure that sufficient numbers could be reisolated for secondary transplants. Secondary engraftment of GFP$^+$ MuSCs isolated from primary recipient muscles after transplant of MuSCs from aged mice was significantly less than for recipients of MuSCs from young mice (**Fig. 1i**,**j** and **Supplementary Fig. 2c**). These findings demonstrate that the regenerative capacity of serially transplanted MuSCs from aged mice is diminished relative to that of MuSCs from young mice, in agreement with findings for hematopoietic stem cells from aged mice[29]. Notably, these results confirm that the intrinsic defects in MuSCs from aged mice are not corrected upon transplantation into a muscle tissue environment of a young mouse and that only a subset of the MuSC population in aged mice retains the long-term functional capacity to reconstitute the stem cell reservoir *in vivo*.

Molecular and cellular changes in MuSCs from aged mice

We sought to identify molecular defects in MuSCs from aged mice that could be targeted therapeutically to enhance their function.

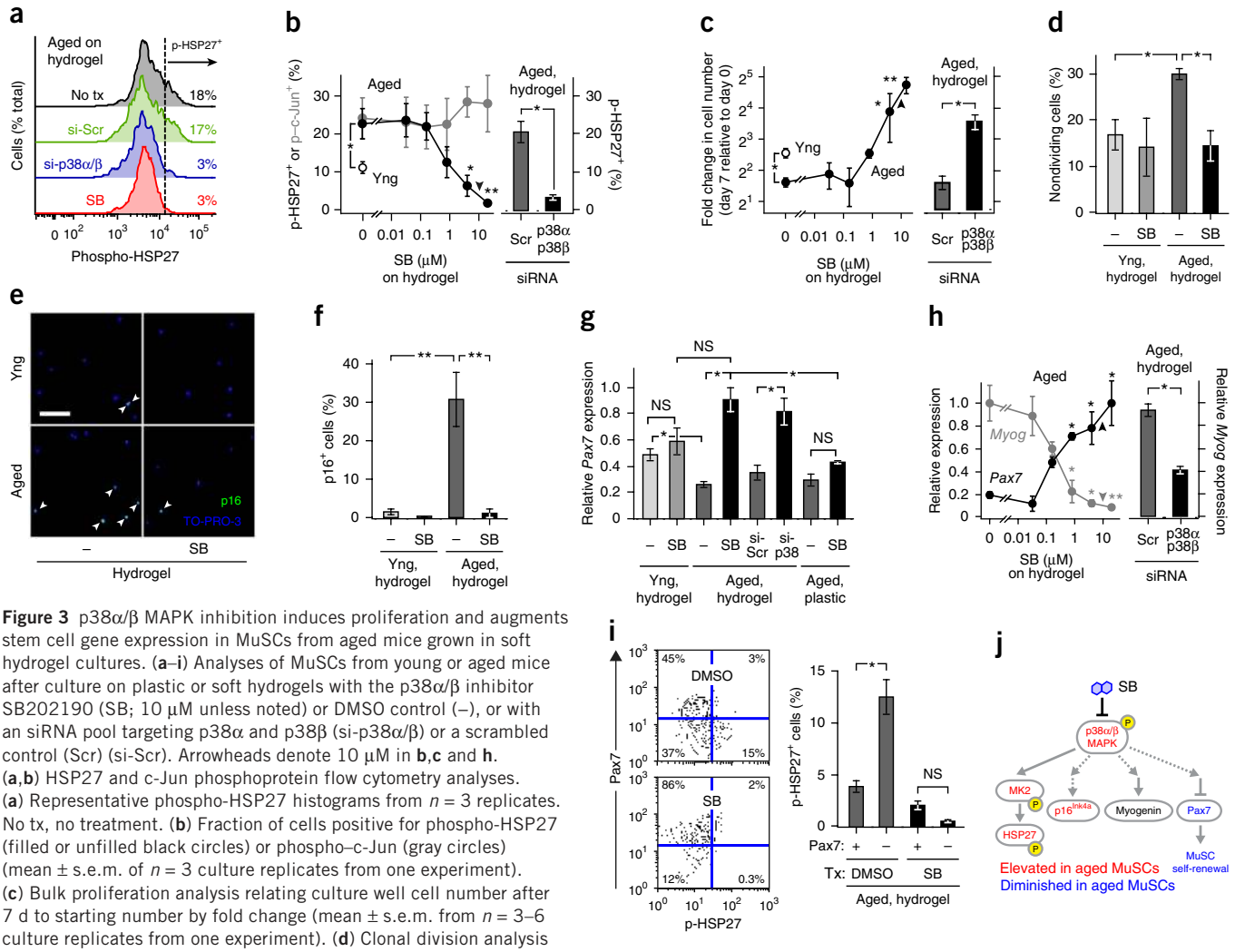

Figure 3 p38α/β MAPK inhibition induces proliferation and augments stem cell gene expression in MuSCs from aged mice grown in soft hydrogel cultures. (**a**–**i**) Analyses of MuSCs from young or aged mice after culture on plastic or soft hydrogels with the p38α/β inhibitor SB202190 (SB; 10 μM unless noted) or DMSO control (–), or with an siRNA pool targeting p38α and p38β (si-p38α/β) or a scrambled control (Scr) (si-Scr). Arrowheads denote 10 μM in **b**,**c** and **h**. (**a**,**b**) HSP27 and c-Jun phosphoprotein flow cytometry analyses. (**a**) Representative phospho-HSP27 histograms from $n = 3$ replicates. No tx, no treatment. (**b**) Fraction of cells positive for phospho-HSP27 (filled or unfilled black circles) or phospho–c-Jun (gray circles) (mean ± s.e.m. of $n = 3$ culture replicates from one experiment). (**c**) Bulk proliferation analysis relating culture well cell number after 7 d to starting number by fold change (mean ± s.e.m. from $n = 3$–6 culture replicates from one experiment). (**d**) Clonal division analysis (mean ± s.e.m. of $n = 4$ experiments). (**e**,**f**) $p16^{Ink4a}$ immunostaining analysis. (**e**) Representative images from $n = 4$ replicates. Arrowheads, positive cells. Scale bar, 100 μm. (**f**) Fraction of cells expressing $p16^{Ink4a}$ (mean ± s.e.m. of $n = 4$ culture replicates). (**g**,**h**) RT-qPCR analysis of *Pax7* and *Myog* expression. (**g**) Mean ± s.e.m. of $n = 6$ culture replicates from two experiments. (**h**) Mean ± s.e.m. of $n = 3$ culture replicates from one experiment. (**i**) Flow cytometric analysis of Pax7 and phospho-HSP27. Left, representative scatter plots from $n = 3$ replicates. Right, p-HSP27$^+$ incidence in Pax7$^+$ and Pax7$^-$ fractions (mean ± s.e.m. of $n = 3$ culture replicates from one experiment). $^*P < 0.05$ or $^{**}P < 0.01$ for conditions different than control by *t*-test (**b**–**d**,**f**–**i**). (**j**) Summary of SB effects on MuSCs from aged mice in hydrogel cultures. MK2, MAP kinase–activated protein kinase 2.

We assayed single cells by nested RT-PCR[11] for their expression of signature MuSC genes[30,31] and found that MuSCs from young and aged mice were similarly highly enriched for stem cells expressing *Pax7* and *Myf5* but not *Pax3* and *Myod1* (**Fig. 2a** and **Supplementary Fig. 3a**). These similar expression profiles suggested that the differences between MuSCs isolated from young and aged mice were not attributable to differences in the purity of the isolated cell population. A conundrum in propagating adult MuSCs *ex vivo* is that MuSCs rapidly lose their stem cell function when cultured on standard tissue culture plastic (1×10^6-kPa rigidity)[11,22,32,33]. We previously showed that this problem can be overcome and stem cell function can be retained if MuSCs are maintained on soft porous hydrogel substrates that are both conjugated with the MuSC niche protein laminin and have a rigidity (12 kPa) similar to skeletal muscle tissue[32,33]. We compared the clonal cell division capacity of MuSCs from young and aged mice in hydrogel microwells and observed that a higher proportion of the MuSCs from aged mice (33%) were unable to divide in mitogenic medium relative to the proportion of the MuSCs from young mice (18%) (**Fig. 2b**,**c**), in accordance with previous findings using other culture systems[34–37] and those evaluating aged human myoblasts[38]. This decrease in the proliferative potential of MuSCs from aged mice was not due to differential survival, as we observed no difference in the viability of MuSCs from young and aged mice (**Supplementary Fig. 3b**).

We observed by immunocytochemical analyses that expression of the cell cycle inhibitors $p16^{Ink4a}$ and $p21^{Cip1}$, two hallmarks of aging-associated cell senescence[29], was higher in freshly FACS-purified MuSCs from aged mice (19%) than in MuSCs from young mice (0.3%) (**Fig. 2d**,**e**). Expression of these senescence factors can be induced by persistent activation of cellular stress–related pathways[39–41]. By assaying stress signaling pathways by phosphoprotein flow cytometric analysis, we found that greater proportions of MuSCs from aged mice (25%), relative to those from young mice (2%), exhibited active p38α/β MAPK signaling (**Fig. 2f**,**g**). These data revealed aberrant p38α/β MAPK signaling as a potential therapeutic target in MuSCs from aged mice.

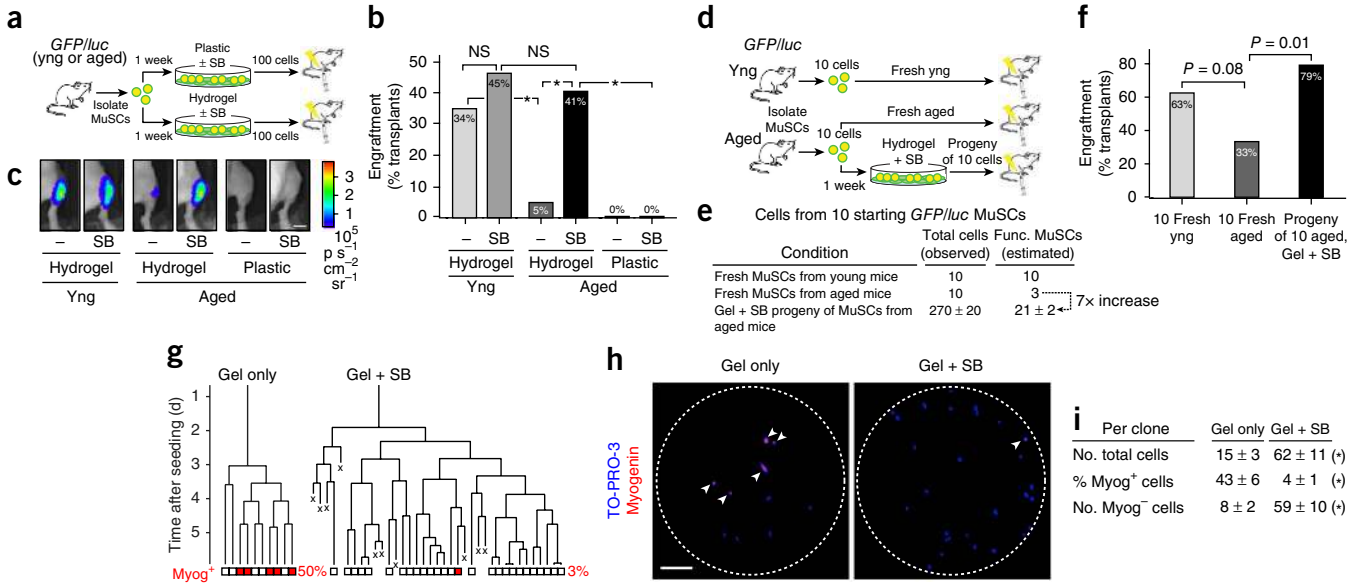

Figure 4 p38α/β inhibition and soft hydrogel substrate synergize to increase the total yield of functional aged stem cells. (**a**–**c**) Engraftment analysis of 100-cell transplants of *GFP/luc*–marked MuSCs populations derived from young or aged mice after culture on plastic or hydrogel with SB202190 (SB; 10 μM) or DMSO control (–) into NOD-SCID hindlimbs by BLI. (**a**) Transplantation scheme. (**b**) Percentage of transplants above engraftment threshold ($n = 41$, 44, 63, 32, 10 and 10 per condition from three experiments). (**c**) Representative BLI images. Scale bar, 5 mm. (**d**–**f**) Engraftment analysis of transplants of the total cell yield of 10 MuSCs from aged mice after SB-hydrogel culture compared with 10 freshly isolated MuSCs from young or aged mice. (**d**) Transplant scheme. (**e**) Estimated number of functional (Func.) MuSCs per condition calculated from *GFP/luc* MuSC proliferation in culture ($n = 3$, mean ± s.e.m.) and functional MuSC frequencies calculated in **Supplementary Figure 7b**. Gel, hydrogel. (**f**) Percentage of transplants above engraftment threshold ($n = 24$ from one experiment). (**g**) Representative fate trees for single MuSCs from aged mice in hydrogel culture without or with SB treatment ($n = 64$ and 75 clones from two experiments). 'X' indicates cell death. (**h**) Corresponding myogenin (Myog) immunostaining images. Arrowheads, positive nuclei. Scale bar, 100 μm. Dashed line indicates the microwell boundary. (**i**) Total and myogenin$^-$ cell numbers and percentage of myogenin$^+$ cells per dividing clone (median ± s.e.m.). *$P < 0.05$ or noted by Fisher's exact test (**b**,**f**) or Mann-Whitney *U*-test (**i**).

p38α/β inhibition enhances MuSC proliferation

We postulated that inhibiting p38α/β signaling during culture of MuSCs from aged mice on soft hydrogel substrates could enhance their stem cell function. After 1 week on soft hydrogel substrates, p38α/β signaling activity in cultured MuSCs from aged mice was higher than in cultured MuSCs from young mice, indicating a difference that persists in the same culture environment (**Fig. 3a**,**b**). Treatment of MuSC cultures from aged mice with SB202190 (hereon abbreviated SB), an imidazole-based ATP competitive inhibitor of the α and β isoforms of p38 MAPK, substantially reduced p38α/β signaling to levels below those of cultured MuSCs from young mice in a dose-dependent fashion, with a saturated effect by 25 μM (**Fig. 3b**). In other cell types[42], inhibition of c-Jun N-terminal kinase signaling is an off-target effect of SB. We did not observe any changes to c-Jun N-terminal kinase activity, as assayed by HSP27 phosphorylation, in SB-treated MuSC cultures (**Fig. 3b**). To confirm the specificity of the SB-mediated effects, we transiently knocked down p38α and p38β with isoform-specific siRNAs (**Supplementary Fig. 4a**,**b**). When we delivered the two siRNAs together, we achieved efficacious knockdown of both *Mapk14* (encoding p38α) and *Mapk11* (encoding p38β) expression (**Supplementary Fig. 4c**,**d**). The combined p38α/β siRNA treatment demonstrated a decrease in phospho-HSP27$^+$ cell frequency in MuSC cultures from aged mice, providing further confirmation of the targets of SB (**Fig. 3a**,**b**).

Transient (1-week) SB treatment alleviated the proliferative defect in MuSCs from aged mice in a concentration-dependent manner (**Fig. 3c** and **Supplementary Fig. 5**). A 1-week SB treatment of MuSCs from aged mice yielded a 35-fold increase in cumulative cell number relative to the starting population, and we observed a similar change in cell number for SB-treated MuSCs from young mice. The proliferative enhancement due to p38α/β inhibition was more pronounced in the MuSCs from aged mice compared to those from young mice relative to their respective uninhibited conditions (18-fold and 11-fold higher, respectively; **Supplementary Fig. 5a**,**b**). We also observed a similar enhancement in proliferation of MuSCs from aged mice by p38α/β siRNA treatment in hydrogel cultures (**Fig. 3c**). The proliferative effect was maximal at 10 μM SB, with a reduced effect observed at 25 μM, as previously reported[43] (**Supplementary Fig. 5c**); therefore, we used a 10 μM concentration for all subsequent studies.

In parallel with the marked increase in proliferation and total cell number, the proportion of both nondividing cells and p16^{Ink4a}-expressing cells was lower in the MuSC population from aged mice treated with SB (**Fig. 3d**–**f**). Notably, these changes were not evident for SB-treated MuSCs from young mice. Thus, SB treatment minimizes the incidence of cell cycle–arrested (quiescent and senescent) cells within the culture progeny of MuSC isolated from aged mice.

SB-hydrogel synergy regulates fates of MuSCs from aged mice

To determine whether the molecular phenotype of SB- and hydrogel-treated MuSCs from aged mice was altered in a synergistic manner, we examined expression signatures of MuSCs and of committed myogenic progenitors at the transcriptional and protein levels. Treatment of MuSCs from aged mice with either the SB inhibitor or the combined p38α/β siRNAs yielded increased expression of the muscle stem cell gene *Pax7* and decreased expression of the commitment gene *Myog* (encoding myogenin), as measured by quantitative RT-PCR, but only when the cells were maintained on soft hydrogels (**Fig. 3g**,**h**). Moreover, single-cell RT-PCR and protein

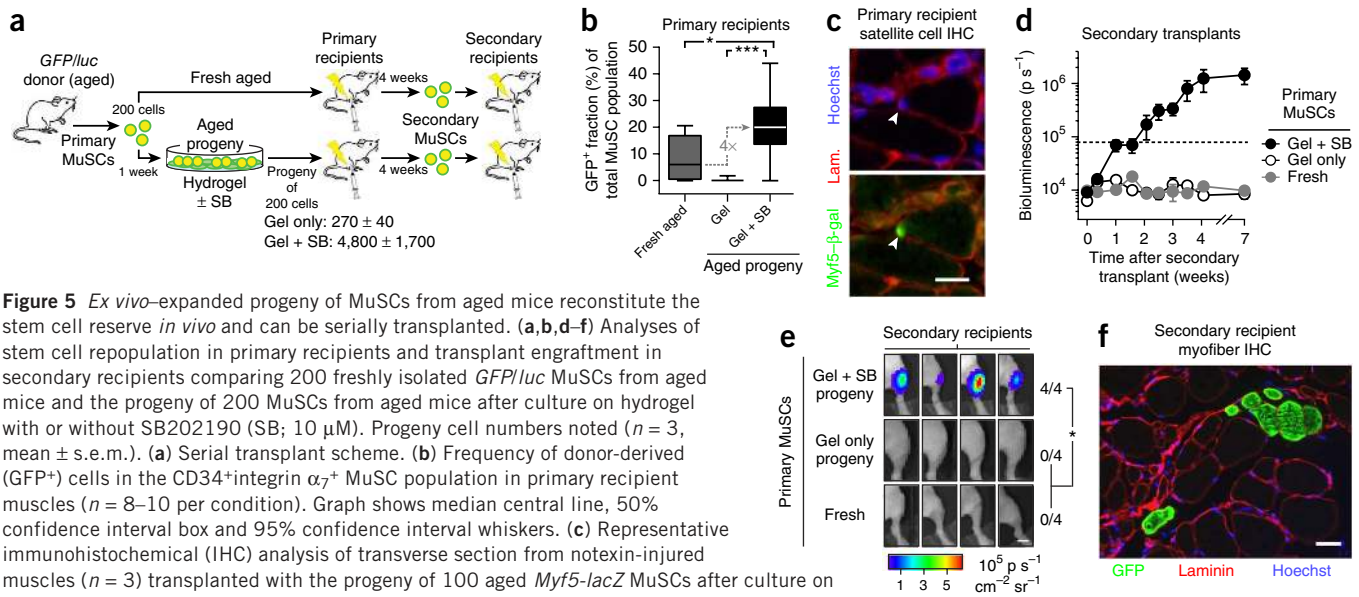

Figure 5 *Ex vivo*–expanded progeny of MuSCs from aged mice reconstitute the stem cell reserve *in vivo* and can be serially transplanted. (**a**,**b**,**d**–**f**) Analyses of stem cell repopulation in primary recipients and transplant engraftment in secondary recipients comparing 200 freshly isolated *GFP/luc* MuSCs from aged mice and the progeny of 200 MuSCs from aged mice after culture on hydrogel with or without SB202190 (SB; 10 μM). Progeny cell numbers noted ($n = 3$, mean ± s.e.m.). (**a**) Serial transplant scheme. (**b**) Frequency of donor-derived (GFP^+) cells in the $CD34^+$integrin α_7^+ MuSC population in primary recipient muscles ($n = 8$–10 per condition). Graph shows median central line, 50% confidence interval box and 95% confidence interval whiskers. (**c**) Representative immunohistochemical (IHC) analysis of transverse section from notexin-injured muscles ($n = 3$) transplanted with the progeny of 100 aged *Myf5-lacZ* MuSCs after culture on hydrogel with 10 μM SB. Arrowheads indicate Myf5–β-galactosidase$^+$ cell in satellite position. Scale bar, 50 μm. Lam., laminin. (**d**–**f**) Engraftment analysis of secondary transplant recipients ($n = 4$). (**d**) BLI signals for up to 2 months after transplant (mean ± s.e.m.). Dashed line represents engraftment detection threshold. (**e**) BLI images at 4 weeks. Engraftment ratios are noted. Scale bar, 5 mm. (**f**) GFP IHC of transverse section representative of $n = 4$ secondary transplant recipients. Primary donor cells were SB-hydrogel progeny of MuSCs from aged mice. Scale bar, 75 μm. $^*P < 0.05$ or $^{***}P < 0.001$ by Student's *t*-test (**b**) or Fisher's exact test (**e**).

flow cytometry assays confirmed that expression of these markers is inversely correlated and that SB treatment promotes a shift in the population of MuSCs from aged mice toward a higher incidence of $Pax7^+$myogenin$^-$ stem cells and fewer $Pax7^-$myogenin$^+$ committed progenitors (**Supplementary Fig. 6**). *Pax7* expression in cultured MuSCs from young mice was not markedly enhanced by SB treatment on hydrogels, suggesting that substrate rigidity has a predominant effect (**Fig. 3g**). By contrast, MuSCs from aged mice that were cultured on hydrogel alone or with SB treatment alone did not exhibit enhanced *Pax7* expression relative to rigid-substrate and no-inhibitor controls, respectively. Thus, maintenance of *Pax7* expression in MuSCs from aged mice required the synergistic interaction of the biophysical and biochemical cues.

A recent report[44] demonstrated that MuSC self-renewal divisions are associated with an asymmetric distribution of active p38α/β signaling components into more committed progeny cells. In accordance with those findings, we observed that the committed progenitors in the progeny of MuSCs from aged mice are those with elevated p38α/β signaling activity (**Fig. 3i**). Taken together, these observations show that MuSCs from aged mice require synergistic biophysical (hydrogel substrate) and biochemical (p38α/β inhibitor) cues in order to augment stem cell gene expression (**Fig. 3j**).

Regenerative potential of MuSCs from aged mice is restored

To determine whether the synergistic effects of p38α/β inhibition and soft hydrogel substrates that led to stem cell marker expression *ex vivo* also altered stem cell function *in vivo*, we tested the regenerative capacity of treated MuSC populations from young and aged mice after transient culture. We exposed MuSC populations isolated from young and old mice to diverse culture conditions for 1 week and then transplanted equivalent numbers (100 cells) into the hindlimbs of young (2 months old) NOD-SCID mice. To compare the proportion of cells from each population with stem cell regenerative capacity, we assessed transplant engraftment by BLI and analyzed these data using the limiting-dilution model (**Fig. 4a**–**c** and **Supplementary Fig. 7**).

After culture on the hydrogel alone, we observed a substantial difference between MuSC populations from young (34% transplant engraftment frequency) and aged (5%) mice (**Fig. 4b**,**c**). Although SB exposure did not significantly alter engraftment of MuSCs from young mice (45%), it significantly enhanced the engraftment of MuSCs from aged mice (41%) to a level similar to that of MuSC populations isolated from young mice and grown in hydrogel culture alone. We confirmed these findings using an alternate p38α/β inhibitor, BIRB 796 (**Supplementary Fig. 7a**). Thus, the combination of biophysical and biochemical cues raised the proportion of MuSCs with regenerative function within the population from aged mice to be equivalent to that of the MuSC population in culture that had been isolated from young mice (**Supplementary Fig. 7b**).

Yield of functional MuSCs from aged mice is increased

Given the greatly enhanced proportion of MuSCs with proliferative (**Fig. 3c**,**d**) and regenerative capacity observed previously (**Fig. 4b**,**c**), we asked whether the synergistic SB-hydrogel treatment could yield a cumulative number of functional stem cells in culture that exceeded that of the freshly purified uncultured MuSC population from aged mice. Such a result would demonstrate that expansion of the functional population had occurred *ex vivo*. We predicted the extent of *ex vivo* expansion by combining the proliferation and limiting-dilution engraftment analyses and estimated that SB-hydrogel treatment induces an average sixfold increase (95% confidence interval range 3- to 17-fold) in functional stem cell numbers in the population from aged mice (**Supplementary Fig. 7b**). To test this possibility, we compared equal numbers (ten cells) of freshly isolated MuSCs from young mice and freshly isolated MuSCs from aged mice to the progeny of ten MuSCs isolated from aged mice after 1 week of SB-hydrogel culture in transplantation assays (**Fig. 4d**,**e**). Transplantation of freshly isolated MuSCs from aged mice resulted in a 33% engraftment frequency, whereas transplantation of the SB-hydrogel culture progeny (a yield of 270 total cells) resulted in engraftment (79%) similar to that of freshly isolated MuSCs from young mice (63%; **Fig. 4e**,**f**).

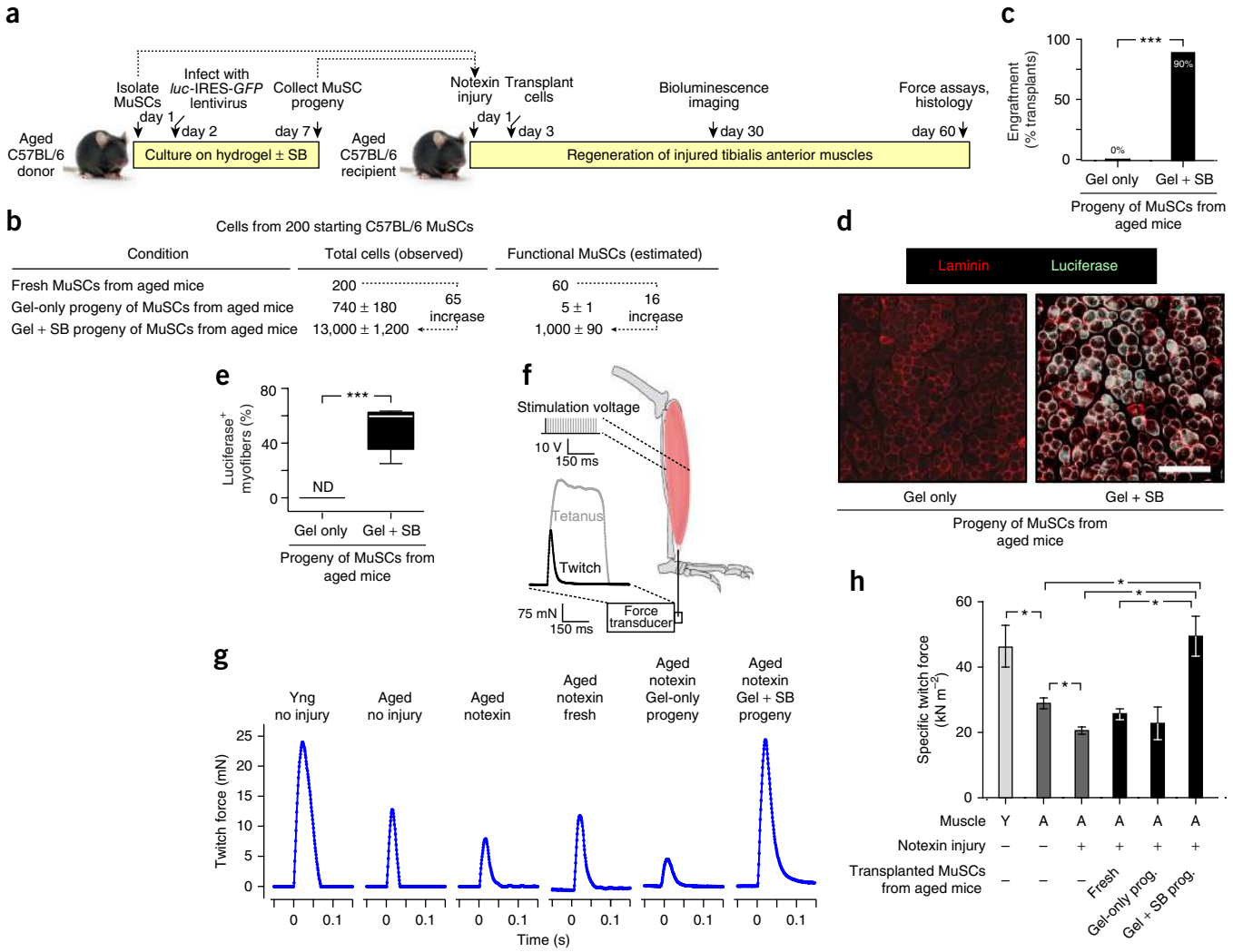

Figure 6 Muscle strength restored in injured aged mice by transplantation of *ex vivo*–expanded progeny of MuSCs from aged mice. (**a**–**e**) Engraftment analysis of 200 fresh C57BL/6 MuSCs from aged mice or their progeny after culture on hydrogel with or without SB202190 (SB; 10 μM) transplanted into the mice of syngeneic injured aged mice. (**a**) Transplant scheme. (**b**) Estimated number of functional MuSCs per condition based on C57BL/6 MuSC proliferation in culture ($n = 3$, mean ± s.e.m.) and functional MuSC frequencies calculated in **Supplementary Figure 7b**. (**c**) Transplant engraftment frequency from BLI ($n = 10$ recipients from two experiments). (**d**,**e**) Luciferase immunohistochemistry in transverse muscle sections ($n = 7$ per condition). (**d**) Representative images with anti-luciferase antibody stain. Scale bar, 500 μm. (**e**) Percentage of luciferase$^+$ myofibers with median central line, 50% confidence interval box and 95% confidence interval whiskers. ND, none detected. (**f**) *In vivo* muscle contractile force assay scheme. (**g**,**h**) Muscle twitch forces in young (Y) and aged (A) mice, without (–) or with (+) notexin injury and subsequent transplantation of freshly isolated MuSCs from aged mice or their culture progeny ($n = 5$ muscles per condition). (**g**) Representative raw force traces. (**h**) Specific muscle twitch forces (mean ± s.e.m.). Prog., progeny. $^*P < 0.05$ or $^{***}P < 0.001$ by Fisher's exact test (**c**), Mann-Whitney *U*-test (**e**) or Student's *t*-test (**h**).

The improved transplant engraftment frequency of the SB-hydrogel progeny provides evidence of a rapid expansion of the functional stem cell population from aged mice.

To determine the basis for the stem cell expansion of the MuSC population from aged mice, we performed single-cell fate analyses of these MuSCs, which is critical given the inherent heterogeneity in MuSC populations[11,18,21,22,27,32]. We established a clonal stem cell fate assay by culturing single MuSCs in hydrogel 'microwells' and analyzing their proliferative behavior by long-term time-lapse microscopy using the automated Baxter cell tracking and lineage reconstruction algorithm[32] paired with an immunocytochemical assay of myogenic differentiation (**Fig. 4g**–**i**). This single-cell analysis revealed that SB treatment led not only to a higher number of the MuSCs from aged mice that gave rise to clones (**Fig. 3d**) but also and more profoundly to a greater number of cells within each of these clones. Furthermore, SB treatment significantly prevented differentiation, as assessed by myogenin expression, indicating a clonal expansion in uncommitted (myogenin$^-$) stem cells (**Fig. 4h**,**i**). Together, these single-cell observations and *in vivo* functional data (**Fig. 4d**–**f**) indicate that the SB and hydrogel treatments act synergistically to stimulate extensive proliferation without differentiation, suggesting that expansion of MuSCs from aged mice occurs by self-renewal.

Long-term function of aged MuSC population is rejuvenated

The repeated capacity to regenerate tissue is an essential characteristic of long-term stem cell function[11,33], which we observed to be defective in MuSCs from aged mice compared to those from young mice (**Fig. 1g**–**j** and **Supplementary Fig. 2c**). The reconstitution of the

functional stem cell reserve *in vivo* by 200 freshly isolated MuSCs from aged *GFP/luc* transgenic mice or their hydrogel culture progeny with or without SB treatment was compared by flow cytometric, immunohistochemical and serial transplant assays (**Fig. 5a–f**). We reisolated and quantified GFP$^+$ MuSCs from the muscles of primary recipient mice (**Fig. 5b**) and transplanted them into secondary recipients (**Fig. 5d–f**). We observed that the SB-hydrogel progeny transplants resulted in an enhanced stem cell reconstitution, as evidenced by a greater proportion of donor-derived (median 21% GFP$^+$) MuSCs in primary transplant recipients compared to that of freshly isolated MuSCs from aged mice (5% GFP$^+$) or the progeny from hydrogel-only culture transplants (0% GFP$^+$; **Fig. 5b**). To assay stem cell niche occupancy by transplanted cells, we isolated MuSCs from transgenic FVB mice with *lacZ* knocked into one allele of the *Myf5* gene (*Myf5-lacZ*), which is expressed only by activated MuSCs but not their committed progeny[11,45]. Histological analysis confirmed that MuSCs from aged *Myf5-lacZ* mice expanded *ex vivo* by SB-hydrogel treatment home to the native niche 1 month following transplantation to replenish the long-term stem cell reserve (**Fig. 5c**). Moreover, these cells are capable of responding to subsequent regenerative demands in transplant recipients, as evidenced by the activation of *Myf5* expression upon notexin damage[11,22,32,45].

Furthermore, compared to freshly isolated MuSCs from aged mice, which have diminished capacity to regenerate muscles upon serial transplant (see **Fig. 1i,j**), the progeny of MuSCs from aged mice that were cultured on SB-treated hydrogel substrates can be serially transplanted, yielding robust and stable engraftment and GFP$^+$ myofibers in secondary recipients (**Fig. 5d–f**). Thus, this MuSC population overcomes the defect in long-term cell repopulation seen with freshly isolated cells from aged mice, providing further evidence of *ex vivo* expansion of the functional stem cell population.

Rejuvenated MuSC population strengthens aged muscles

We developed a preclinical model of autologous cell therapy to evaluate whether SB-treated MuSC populations from aged mice could regenerate the injured muscles of aged mice. The experiments described above (**Figs. 1**, **4** and **5**) all used immunocompromised young NOD-SCID recipients. In contrast, here we evaluated MuSCs from aged mice transplanted into syngeneic age-matched C57BL/6 wild-type recipients 2 d following local notexin injury (**Fig. 6a**). We compared the soft hydrogel culture progeny of 200 MuSCs from aged mice (without or with SB treatment, which proliferated extensively to yield 740 and 13,000 total cells per transplant, respectively; **Fig. 6b**). We infected cells with a lentivirus encoding both luciferase and GFP for engraftment analyses. Transplants of SB-treated progeny of MuSCs from aged mice engrafted at a high frequency (90%) even in aged wild-type recipient mice, whereas hydrogel-only grown progeny of MuSCs from aged mice did not engraft at all (0%; **Fig. 6c**). Moreover, the transplanted SB-treated progeny contributed to the repair of a high proportion (63%; **Fig. 6d,e**) of recipient myofibers, as assessed by luciferase immunohistochemistry, which is probably a substantial underrepresentation given that only 33% of cells were labeled by the lentiviral luciferase transgene before transplantation (**Supplementary Fig. 8a**). These data suggest that the expanded MuSC population from aged mice had increased to a number that was effective in repairing the majority of myofibers in injured muscles in aged mice.

As the ultimate test of functional recovery, we determined whether the delivery of *ex vivo* SB-treated progeny of MuSCs from aged mice could restore muscle strength to notexin-injured aged recipients 1 month after transplant. To avoid potential artifacts associated with measurements that entail complete muscle excision and rigor mortis, we assayed specific twitch and tetanus force generation in intact tibialis anterior muscles in live anesthetized mice[46,47] (**Fig. 6f**). Compared to muscles of young mice, muscles of aged mice exhibited reduced twitch forces, whereas tetanus forces were similar for both (**Fig. 6g,h** and **Supplementary Fig. 8b–d**). These observations are in agreement with prior reports that a reduction in fast-twitch (type II) rather than slow-twitch (type I) fibers is observed with aging[48]. Injured muscles of aged mice exhibited defective regeneration, which was evident by both impaired twitch and tetanus force generation, as expected[2]. Transplantation of freshly isolated MuSCs from aged mice resulted in a minor recovery in twitch force. By contrast, injured muscles of aged mice that received transplants of the SB-hydrogel–treated progeny of MuSCs from aged mice exhibited increases in both twitch and tetanus forces that restored them to the levels found in uninjured muscles of young mice. The cell numbers required are consistent with a recent report that 900 or more functional MuSCs from young mice are necessary and sufficient to achieve tibialis anterior strength recovery in a dystrophic mouse model[49]. Our findings provide evidence of the potent restorative function of the expanded MuSC population derived from aged mice, even in an injured aged syngeneic and immunocompetent recipient.

DISCUSSION

Here we present evidence that MuSCs from aged mice differ intrinsically from their counterparts in young mice and provide a strategy to rejuvenate the function of MuSCs from the aged mice. We demonstrate that MuSCs from aged mice have cell-autonomous self-renewal defects that lead to impaired regeneration, stem cell repopulation and serial transplantation *in vivo*, which are not corrected even when transplanted into young mice. These findings show not only that the previously described extrinsic systemic and tissue microenvironmental changes[15,17] have marked effects but also that factors intrinsic to MuSCs change and impair muscle regeneration with aging. Given the rarity of stem cells in muscle tissues, the determination that stem cell populations from muscles of aged mice have lost two-thirds of the functional capacity of those from young mice constitutes a major challenge for stem cell–based therapies in the elderly. However, this observation also provides a previously unrecognized opportunity to identify cell-intrinsic molecular changes that can be targeted to increase the number of fully functional stem cells in order to develop an autologous stem cell therapy for the elderly.

We show that a greater proportion of muscle stem cells from aged mice exhibit persistently elevated p38α/β MAPK activity and expression of the cell cycle inhibitors p16^{Ink4a} and p21^{Cip1} compared to MuSCs from young mice. p38α/β signaling inhibits MuSC gene expression, promotes myoblast differentiation, and is required for muscle regeneration[43,44,50–52]. In agreement with our findings in muscle, other studies have shown that p38α/β signaling induces p16^{Ink4a} expression and promotes cell senescence in human fibroblasts[41] and that its inhibition can extend the proliferative lifespan of fibroblasts[53], pancreatic islet cells[37] and hematopoietic stem cells[40,54]. Others have noted that activated satellite cells retain phosphorylated p38α/β (ref. 44) and satellite cells from aged mice have a more 'activated' phenotype *in vivo*[19]. Here we extend these findings by showing that MuSCs from aged mice manifest an intrinsic difference in p38α/β signaling.

We show that the synergistic action of a biophysical cue (substrate rigidity) and a biochemical cue (p38α/β signaling inhibitor)

is required to rejuvenate the cumulative MuSC population after their isolation from aged mice. Neither of these factors alone is efficacious in enhancing MuSC *Pax7* expression and transplant engraftment of these cells. In contrast, the biophysical cue of substrate rigidity predominates for MuSCs from young mice, as might be expected given their minimal p38α/β activity. Thus, the observed synergistic effects on *ex vivo* self-renewal are specific to MuSCs from aged mice.

Our findings demonstrate that active p38α/β is a potent target for directed and rapid expansion of functional stem cells from muscle tissues of aged mice when administered in the context of soft hydrogel. The progeny derived from SB-treated hydrogel cultures after 1 week increased 30- to 60-fold (dependent on mouse strain) and had improved function over the freshly isolated stem cells from aged mice. This provides evidence of *ex vivo* expansion of the residual one-third of the MuSC population that remains functional with aging. Time-lapse analysis revealed that this was primarily due to the increase in progeny in a subset of clones. Notably, this *ex vivo*–expanded MuSC population from aged mice conferred long-term beneficial effects *in vivo* in mice, as the cells exhibited enhanced repopulation of the stem cell reservoir and function in serial transplants. To our knowledge, this is the first strategy reported for rapid and directed functional stem cell expansion from muscle tissues of aged mice. Notably, the expanded MuSC population from aged mice contributed to extensive myofiber repair and restored strength to injured muscles in aged mice.

Adult stem cells are advantageous for regenerative medicine, as they have a known identity, integrate well within the tissue following delivery and are committed to regenerating their tissue of origin. Moreover, their potential for tumorigenicity is low, as skeletal muscle tumors (rhabdomyosarcoma) are very rare in adults[55]. Treatment *ex vivo* avoids possible side effects within other tissues that could result when small-molecule inhibitors[56] or siRNAs are delivered systemically. Our findings provide a new approach for rapid and marked expansion of functional MuSCs *ex vivo* by short-term treatment in culture, which provides a paradigm for an autologous muscle stem cell therapy for restoring strength in cases of localized muscle damage in the elderly.

METHODS

Methods and any associated references are available in the online version of the paper.

Note: Any Supplementary Information and Source Data files are available in the online version of the paper.

ACKNOWLEDGMENTS

We thank K. Koleckar, P. Kraft, N. Nguyen, A. Thayer, C. Marceau, K. Magnusson and A. Ho for technical assistance; K. Havenstrite and R. Haynes for polymer synthesis; and the Stanford Center for Innovation in In-Vivo Imaging (SCI[3]), the Stanford Shared FACS Facility (SSFF) and IBM Almaden for technical support. This work was funded by US National Institutes of Health (NIH) training grant R25CA118681 and grant K99AG042491 (B.D.C.); NIH training grant T32CA009151 and grant K99AR061465 and California Institute for Regenerative Medicine training grant TG2-01159 (P.M.G.); and NIH grants U01HL100397, U01HL099997, R01AG020961, R01HL096113 and R01AG009521, an IBM Faculty Award, California Institute for Regenerative Medicine grants RT1-01001 and TR3-05501 and the Baxter Foundation (H.M.B.).

AUTHOR CONTRIBUTIONS

B.D.C., P.M.G. and E.P. designed and performed experiments, analyzed data and wrote the manuscript. F.M., S.P.L., S.Y.C. and M.E.L. developed methods, performed experiments and analyzed data. S.L.D. developed methods and wrote the manuscript. H.M.B. designed experiments, analyzed data and wrote the manuscript.

COMPETING FINANCIAL INTERESTS

The authors declare no competing financial interests.

1. Ryall, J.G., Schertzer, J.D. & Lynch, G.S. Cellular and molecular mechanisms underlying age-related skeletal muscle wasting and weakness. *Biogerontology* **9**, 213–228 (2008).
2. Grounds, M.D. Age-associated changes in the response of skeletal muscle cells to exercise and regeneration. *Ann. NY Acad. Sci.* **854**, 78–91 (1998).
3. Benny Klimek, M.E. *et al.* Acute inhibition of myostatin-family proteins preserves skeletal muscle in mouse models of cancer cachexia. *Biochem. Biophys. Res. Commun.* **391**, 1548–1554 (2010).
4. Di Marco, S. *et al.* The translation inhibitor pateamine A prevents cachexia-induced muscle wasting in mice. *Nat. Commun.* **3**, 896 (2012).
5. Sandri, M. *et al.* Foxo transcription factors induce the atrophy-related ubiquitin ligase atrogin-1 and cause skeletal muscle atrophy. *Cell* **117**, 399–412 (2004).
6. Stitt, T.N. *et al.* The IGF-1/PI3K/Akt pathway prevents expression of muscle atrophy-induced ubiquitin ligases by inhibiting FOXO transcription factors. *Mol. Cell* **14**, 395–403 (2004).
7. Glass, D. & Roubenoff, R. Recent advances in the biology and therapy of muscle wasting. *Ann. NY Acad. Sci.* **1211**, 25–36 (2010).
8. Sakuma, K. & Yamaguchi, A. Molecular mechanisms in aging and current strategies to counteract sarcopenia. *Curr. Aging Sci.* **3**, 90–101 (2010).
9. Janssen, I., Shepard, D.S., Katzmarzyk, P.T. & Roubenoff, R. The healthcare costs of sarcopenia in the United States. *J. Am. Geriatr. Soc.* **52**, 80–85 (2004).
10. Mauro, A. Satellite cell of skeletal muscle fibers. *J. Biophys. Biochem. Cytol.* **9**, 493–495 (1961).
11. Sacco, A., Doyonnas, R., Kraft, P., Vitorovic, S. & Blau, H.M. Self-renewal and expansion of single transplanted muscle stem cells. *Nature* **456**, 502–506 (2008).
12. Brack, A.S. & Rando, T.A. Tissue-specific stem cells: lessons from the skeletal muscle satellite cell. *Cell Stem Cell* **10**, 504–514 (2012).
13. Brack, A.S. & Rando, T.A. Intrinsic changes and extrinsic influences of myogenic stem cell function during aging. *Stem Cell Rev.* **3**, 226–237 (2007).
14. Gopinath, S.D. & Rando, T.A. Stem cell review series: aging of the skeletal muscle stem cell niche. *Aging Cell* **7**, 590–598 (2008).
15. Brack, A.S. *et al.* Increased Wnt signaling during aging alters muscle stem cell fate and increases fibrosis. *Science* **317**, 807–810 (2007).
16. Conboy, I.M., Conboy, M.J., Smythe, G.M. & Rando, T.A. Notch-mediated restoration of regenerative potential to aged muscle. *Science* **302**, 1575–1577 (2003).
17. Conboy, I.M. *et al.* Rejuvenation of aged progenitor cells by exposure to a young systemic environment. *Nature* **433**, 760–764 (2005).
18. Collins, C.A., Zammit, P.S., Ruiz, A.P., Morgan, J.E. & Partridge, T.A. A population of myogenic stem cells that survives skeletal muscle aging. *Stem Cells* **25**, 885–894 (2007).
19. Carlson, M.E., Hsu, M. & Conboy, I.M. Imbalance between pSmad3 and Notch induces CDK inhibitors in old muscle stem cells. *Nature* **454**, 528–532 (2008).
20. Chakkalakal, J.V., Jones, K.M., Basson, M.A. & Brack, A.S. The aged niche disrupts muscle stem cell quiescence. *Nature* **490**, 355–360 (2012).
21. Cerletti, M. *et al.* Highly efficient, functional engraftment of skeletal muscle stem cells in dystrophic muscles. *Cell* **134**, 37–47 (2008).
22. Kuang, S., Kuroda, K., Le Grand, F. & Rudnicki, M.A. Asymmetric self-renewal and commitment of satellite stem cells in muscle. *Cell* **129**, 999–1010 (2007).
23. Montarras, D. *et al.* Direct isolation of satellite cells for skeletal muscle regeneration. *Science* **309**, 2064–2067 (2005).
24. Cornelison, D.D. *et al.* Essential and separable roles for syndecan-3 and syndecan-4 in skeletal muscle development and regeneration. *Genes Dev.* **18**, 2231–2236 (2004).
25. Bosnakovski, D. *et al.* Prospective isolation of skeletal muscle stem cells with a Pax7 reporter. *Stem Cells* **26**, 3194–3204 (2008).
26. Lefkovits, I. & Waldmann, H. *Limiting dilution analysis of cells of the immune system* (Oxford University Press, Oxford, 1999).
27. Rocheteau, P., Gayraud-Morel, B., Siegl-Cachedenier, I., Blasco, M.A. & Tajbakhsh, S. A subpopulation of adult skeletal muscle stem cells retains all template DNA strands after cell division. *Cell* **148**, 112–125 (2012).
28. Darabi, R. *et al.* Assessment of the myogenic stem cell compartment following transplantation of Pax3/Pax7-induced embryonic stem cell–derived progenitors. *Stem Cells* **29**, 777–790 (2011).
29. Rossi, D.J., Jamieson, C.H. & Weissman, I.L. Stems cells and the pathways to aging and cancer. *Cell* **132**, 681–696 (2008).
30. Seale, P. *et al.* Pax7 is required for the specification of myogenic satellite cells. *Cell* **102**, 777–786 (2000).
31. Kang, J.S. & Krauss, R.S. Muscle stem cells in developmental and regenerative myogenesis. *Curr. Opin. Clin. Nutr. Metab. Care* **13**, 243–248 (2010).
32. Gilbert, P.M. *et al.* Substrate elasticity regulates skeletal muscle stem cell self-renewal in culture. *Science* **329**, 1078–1081 (2010).
33. Cosgrove, B.D., Sacco, A., Gilbert, P.M. & Blau, H.M. A home away from home: challenges and opportunities in engineering *in vitro* muscle satellite cell niches. *Differentiation* **78**, 185–194 (2009).
34. Shefer, G., Van de Mark, D.P., Richardson, J.B. & Yablonka-Reuveni, Z. Satellite-cell pool size does matter: defining the myogenic potency of aging skeletal muscle. *Dev. Biol.* **294**, 50–66 (2006).

35. Schultz, E. & Lipton, B.H. Skeletal muscle satellite cells: changes in proliferation potential as a function of age. *Mech. Ageing Dev.* **20**, 377–383 (1982).
36. Mouly, V. *et al.* The mitotic clock in skeletal muscle regeneration, disease and cell mediated gene therapy. *Acta Physiol. Scand.* **184**, 3–15 (2005).
37. García-Prat, L., Sousa-Victor, P. & Munoz-Canoves, P. Functional dysregulation of stem cells during aging: a focus on skeletal muscle stem cells. *FEBS J.* **280**, 4051–4062 (2013).
38. Beccafico, S. *et al.* Human muscle satellite cells show age-related differential expression of S100B protein and RAGE. *Age* (*Dordr.*) **33**, 523–541 (2011).
39. Wong, E.S. *et al.* p38MAPK controls expression of multiple cell cycle inhibitors and islet proliferation with advancing age. *Dev. Cell* **17**, 142–149 (2009).
40. Ito, K. *et al.* Reactive oxygen species act through p38 MAPK to limit the lifespan of hematopoietic stem cells. *Nat. Med.* **12**, 446–451 (2006).
41. Iwasa, H., Han, J. & Ishikawa, F. Mitogen-activated protein kinase p38 defines the common senescence-signalling pathway. *Genes Cells* **8**, 131–144 (2003).
42. Bain, J. *et al.* The selectivity of protein kinase inhibitors: a further update. *Biochem. J.* **408**, 297–315 (2007).
43. Jones, N.C. *et al.* The p38α/β MAPK functions as a molecular switch to activate the quiescent satellite cell. *J. Cell Biol.* **169**, 105–116 (2005).
44. Troy, A. *et al.* Coordination of satellite cell activation and self-renewal by Par-complex-dependent asymmetric activation of p38α/β MAPK. *Cell Stem Cell* **11**, 541–553 (2012).
45. Tajbakhsh, S. *et al.* Gene targeting the *myf-5* locus with nlacZ reveals expression of this myogenic factor in mature skeletal muscle fibres as well as early embryonic muscle. *Dev. Dyn.* **206**, 291–300 (1996).
46. Sacco, A. *et al.* Short telomeres and stem cell exhaustion model Duchenne muscular dystrophy in mdx/mTR mice. *Cell* **143**, 1059–1071 (2010).
47. Llewellyn, M.E., Thompson, K.R., Deisseroth, K. & Delp, S.L. Orderly recruitment of motor units under optical control *in vivo*. *Nat. Med.* **16**, 1161–1165 (2010).
48. Thompson, L.V. Effects of age and training on skeletal muscle physiology and performance. *Phys. Ther.* **74**, 71–81 (1994).
49. Arpke, R.W. *et al.* A new immuno-, dystrophin-deficient model, the NSG-*mdx*^{4Cv} mouse, provides evidence for functional improvement following allogeneic satellite cell transplantation. *Stem Cells* **31**, 1611–1620 (2013).
50. Lluís, F., Perdiguero, E., Nebreda, A.R. & Munoz-Canoves, P. Regulation of skeletal muscle gene expression by p38 MAP kinases. *Trends Cell Biol.* **16**, 36–44 (2006).
51. Palacios, D. *et al.* TNF/p38α/polycomb signaling to Pax7 locus in satellite cells links inflammation to the epigenetic control of muscle regeneration. *Cell Stem Cell* **7**, 455–469 (2010).
52. Brien, P., Pugazhendhi, D., Woodhouse, S., Oxley, D. & Pell, J.M. p38α MAPK regulates adult muscle stem cell fate by restricting progenitor proliferation during postnatal growth and repair. *Stem Cells* **31**, 1597–1610 (2013).
53. Tivey, H.S. *et al.* Small molecule inhibition of p38 MAP kinase extends the replicative life span of human ATR-Seckel syndrome fibroblasts. *J. Gerontol. A Biol. Sci. Med. Sci.* **68**, 1001–1009 (2013).
54. Zou, J. *et al.* Inhibition of p38 MAPK activity promotes *ex vivo* expansion of human cord blood hematopoietic stem cells. *Ann. Hematol.* **91**, 813–823 (2012).
55. Parham, D.M. & Ellison, D.A. Rhabdomyosarcomas in adults and children: an update. *Arch. Pathol. Lab. Med.* **130**, 1454–1465 (2006).
56. Page, T.H., Brown, A., Timms, E.M., Foxwell, B.M. & Ray, K.P. Inhibitors of p38 suppress cytokine production in rheumatoid arthritis synovial membranes: does variable inhibition of interleukin-6 production limit effectiveness *in vivo*? *Arthritis Rheum.* **62**, 3221–3231 (2010).

ONLINE METHODS

Mice. The Stanford University Administrative Panel on Laboratory Animal Care (APLAC) approved all animal protocols. We performed all experiments in compliance with the institutional guidelines of Stanford University. We purchased C57BL/6 mice from the US National Institute on Aging. Transgenic mice were obtained and maintained as described previously[11]. Mice expressing a green fluorescent protein (*GFP*) transgene under regulation of the ubiquitous *UBC* promoter were maintained in the C57BL/6 strain. Mice expressing a firefly luciferase (*luc*) transgene under regulation of the ubiquitous *Actb* promoter were maintained in the FVB strain. We generated double-transgenic *GFP*/*luc* mice by crossing the above strains as described previously[11]. Mice expressing a β-galactosidase (*lacZ*) transgene inserted into one allele of the *Myf5* gene (*Myf5*-*lacZ*) were maintained in the FVB strain[45]. We validated these genotypes by appropriate PCR-based strategies. We used cells from C57BL/6 mice for cell proliferation, phosphoprotein analysis, gene expression and syngeneic transplant experiments. We used cells from *GFP*/*luc* and *Myf5*-*lacZ* mice for allogenic transplantation experiments into NOD-SCID (Jackson Laboratory) recipient mice. We studied young mice at 2–4 months of age (median 2 months) and aged mice at 22–28 months of age (median 24 months) for all strains and genders. All mice used in these studies were females, except as noted in **Supplementary Figure 1d**.

Muscle stem cell isolation. We isolated and enriched muscle stem as previously described[11]. Briefly, we dissected tibialis anterior and gastrocnemius muscles from mice and subjected them to collagenase (0.25%; Roche) and dispase (0.04 U ml^{-1}; Roche) digestion. After this digestion step, we kept cells at 4 °C until culture or transplantation. We removed nonmuscle tissue under a dissection microscope and then dissociated muscle fibers. After 90 min total digestion, we passed the remaining cell suspension through sequential 70-μm and 40-μm filters (BD Biosciences) to generate single-cell suspensions. We first incubated cells with biotinylated antibodies reactive to CD45 (BD Biosciences, clone 30F11, catalog # 553078, 1:500), CD11b (BD Biosciences, clone M1/70, catalog # 553309, 1:800), CD31 (eBiosciences, clone 390, catalog # 13-0311-82, 1:200) and Sca1 (BD Biosciences, clone E13-161.7, catalog # 553334, 1:200). We then incubated cells with streptavidin magnetic beads (Miltenyi Biotech), streptavidin–Texas Red (Invitrogen, catalog # S872, 1:200), integrin α_7–specific antibody labeled with phycoerythrin (AbLab, clone R2F2, catalog # 10ST215, 1:500) and CD34-specific antibody labeled with eFluor660 (eBioscience, clone RAM34, catalog # 50-0341-82, 1:67).

We magnetically depleted biotin-positive cells on a selection column (Miltenyi). We then sorted the biotin-negative cells on a modified FACStar Plus or FACS Aria cell sorter using FACSDiva software (BD Biosciences). We enriched MuSCs by gating viable cells (propidium iodide–negative) for cells negative for the lineage marker panel (CD45, CD31, CD11b and Sca1) and positive for both CD34 and integrin α_7. We double-sorted cells for purity (routinely >95% for cells from C57BL/6 mice). For cells from *GFP*/*luc* mice, we also gated for GFP positivity and routinely obtained >92% double-sorted purity. We generated and analyzed flow cytometry scatter plots using FlowJo v8.7 (Treestar).

Muscle stem cell transplantation. We transplanted MuSCs immediately following FACS isolation or after collection from cell culture directly into the tibialis anterior muscle of recipient mice as previously described[11,32]. We transplanted cells from *GFP*/*luc* or *Myf5*-*lacZ* mice into gender-matched hindlimb-irradiated NOD-SCID (2–4 months of age, median 2 months) mice (**Figs. 1**, **4** and **5**). Before transplantation, we anesthetized NOD-SCID mice with ketamine (2.4 mg per mouse) and xylazine (240 μg per mouse) by intraperitoneal injection. We then irradiated hindlimbs with a single 18 Gy dose, with the rest of the body was shielded in a lead jig. We performed transplantations within 3 d of irradiation.

In syngeneic studies (**Fig. 6**), we transplanted cells from aged C57BL/6 mice into nonirradiated gender-matched littermate aged C57BL/6 mice (Jackson). For these experiments, aged C57BL/6 MuSCs were exposed to a *luc*-IRES-*GFP* lentivirus at day 2 of culture for a period of 24 h. Two days before cell transplantation, we acutely injured tibialis anterior muscles in recipient aged C57BL/6 mice by a single 10-μl intramuscular injection of notexin (10 μg ml^{-1}; Latoxan).

We collected cells from hydrogel cultures by incubation with 0.5% trypsin in PBS for 2 min at 37 °C and counted them using a hemocytometer. For both FACS-isolated and cultured cells, we washed cells three times and counted them with a hemocytometer. We resuspended cells at desired cell concentrations in PBS with 2.5% goat serum and 1 mM EDTA and then transplanted them by intramuscular injection into the tibialis anterior muscles in a 10-μl volume. We compared cells from different conditions by transplantation into the tibialis anterior muscles of contralateral legs in the same mice.

Bioluminescence imaging. We performed bioluminescence imaging (BLI) using a Xenogen-100 system, as previously described[11]. Briefly, we anesthetized mice using isoflurane and administered 100 μL D-luciferin (0.1 mmol kg^{-1}, reconstituted in PBS; Caliper LifeSciences) by intraperitoneal injection. We analyzed BLI using a 60-s exposure acquired at 12 min after luciferin injection. Digital images were recorded and analyzed using Living Image software (Caliper LifeSciences). We analyzed images with a consistent region-of-interest (ROI) placed over each hindlimb to calculate a bioluminescence signal. We used a bioluminescence signal value of 80,000 photons per second to define an engraftment threshold. This BLI level corresponds to the histological detection of one or more GFP^+ myofibers (see **Supplementary Fig. 1c** and ref. 32). We performed BLI imaging at 1 month after transplantation, unless otherwise stated.

Tissue histology. We collected and prepared recipient tibialis anterior muscle tissues for histology to analyze the expression of donor-cell transgene products as previously described[11,32]. We incubated transverse sections with anti-laminin (Millipore, clone A5, catalog # 05-206, 1:250), anti-GFP (Invitrogen, catalog # A11122, 1:200) and/or anti-luciferase (Abcam, catalog # ab81822, 1:100) primary antibodies and then with AlexaFluor 594–conjugated donkey anti-rat IgG1 and AlexaFluor 488–conjugated donkey anti-rabbit (Jackson ImmunoResearch Laboratories, catalog # 712-585-150 and 711-545-152 respectively, 1:200 each) secondary antibodies. We counterstained nuclei with Hoechst 33342 (Invitrogen) or TO-PRO-3 (Invitrogen). We acquired images with an AxioPlan2 epifluorescent microscope (Carl Zeiss Microimaging, Thornwood, NY) with Plan NeoFluar 10×/0.30NA or 20×/0.75NA objectives (Carl Zeiss) and an ORCA-ER digital camera (Hamamatsu Photonics). We captured digital images in OpenLab software (Improvision) and assembled multipanel figures using Photoshop software (Adobe) with consistent contrast adjustments across all images from the same stain.

Limiting-dilution analysis. To calculate the effective number of functional MuSCs in any transplanted cell population, we related the transplant engraftment efficiency to the number of cells transplanted (across a range of transplanted cell numbers) using an exponential stem cell limiting-dilution model[26].

$$\%\,\text{engraftment} = 100\% \times [1 - \exp[-\beta \times (\text{No. cells transplanted})]]$$

β is an exponential coefficient fit from experimental data and differs for each sample. This model fit well to experimental data from transplants of MuSCs from young and aged mice (R^2 = 0.92–0.99, range; see **Fig. 1f** and **Supplementary Figs. 1e** and **7b**). Using this model, we calculated the absolute number of 'functional' MuSCs (defined as equivalent to freshly isolated MuSCs from young mice) within each sample population.

$$\text{No. functional MuSCs} = (\beta_{\text{sample}}/\beta_{\text{Yng,fresh}}) \times (\text{No. cells})$$

Serial transplantation assay. We transplanted a set number (for example, 700 in **Fig. 1i**,**j** and 200 in **Fig. 5d**–**f**) of freshly isolated MuSCs or a 1-week culture progeny from the same starting number of cells into hindlimb-irradiated NOD-SCID primary recipients. One month after transplant, we collected and digested primary recipient muscles. We reisolated donor cells by gating for cells negative for propidium iodide and the CD45, CD11b, CD31 and Sca1 lineage markers and positive for the donor GFP markers from primary recipient muscle cell digestion by FACS. We gated the GFP^+ cells into two populations by FACS based on their expression of the $CD34^+$integrin α_7^+ MuSC surface marker signature. See **Supplementary Figure 2b** for representative FACS scatter plots for reisolation sorting. To perform secondary transplants, we pooled cells isolated from

multiple primary recipients that received cells from the same condition and distributed them equally among secondary transplant recipients such that the average yield of GFP$^+$ MuSCs collected from each primary transplant recipient was injected into each secondary recipient. One month later, we analyzed these secondary recipients by BLI for transplant engraftment.

Quantification of donor-derived muscle stem cells in transplant recipients. We used flow cytometry to quantify donor-derived (GFP$^+$) MuSCs as a proportion of all CD34$^+$integrin α_7^+ MuSCs in recipient muscles after transplantation with freshly isolated *GFP/luc* MuSCs or their culture progeny. One month after transplant, we assessed transplant engraftment by BLI. The following day, we collected and digested primary transplant recipient tibialis anterior muscles. We labeled and magnetically depleted cell suspensions based on CD45, CD11b, CD31 and Sca1 expression. From this depleted population, we gated for propidium iodide$^-$CD45$^-$CD11b$^-$CD31$^-$Sca1$^-$ cells by FACS. Within this population, we analyzed CD34$^+$integrin α_7^+ cells, representing the entire recipient MuSC population, for GFP positivity (see **Fig. 1g**).

Single-cell RT-PCR. We performed nested multiplexed RT-PCR on freshly sorted single MuSCs or single cells from harvested culture to evaluate muscle stem and progenitor cell phenotypes. We removed cultured cells from substrates by gentle trypsinization with 0.1% trypsin in PBS for 2 min. To select single cells, we plated cell suspensions into hydrogel microwell arrays containing no adhesive interface, as previously described[11]. We picked single cells from arrays using a micromanipulator and then transferred them into a PCR lysis buffer. We performed nested RT-PCR as previously described[11], using the following primers: *Pax7* external, forward 5′-GAGTTCGATTAGCCGAGTGC-3′, reverse 5′-GGTTAGCTCCTGCCTGCTTA-3′; *Pax7* internal, forward 5′-GCGAGAAGAAAGCCAAACAC-3′, reverse 5′-GGGTGTAGATGTCC GGGTAG-3′; *Myf5* external, forward 5′-AGACGCCTGAAGAAGGTCAA-3′, reverse 5′-AGCTGGACACGGAGCTTTTA-3′; *Myf5* internal, forward 5′-C CACCAACC CTAAC CAGAGA-3′, reverse 5′-CTGTTCTTTCGGGACCAG AC-3′; *Pax3* external, forward 5′-AACCATATCCGCCACAAGAT-3′, reverse 5′-CTAGATCCGCCTCCTCCTCT-3′; *Pax3* internal, forward 5′-CCCATGGTTGCGTCTCTAAG-3′, reverse 5′-GGATGCGGCTGATAGA ACTC-3′; *Myod1* external, forward 5′-TACCCAAGGTGGAGATCCTG-3′, reverse 5′-GTGGAGATGCGCTCCACTAT-3′; *Myod1* internal, forward 5′-GCC TTCTACGCACCTGGAC-3′, reverse 5′-ACTCTTCCCTGCCTGGACT-3′; *Myog* external, forward 5′-GAAAGTGAATGAGGCCTTCG-3′, reverse 5′-AC- GATGGACGTAAGGGAGT-3′; and *Myog* internal, forward 5′-CGGCTGC CTAAAGTGGAGAT-3′, reverse 5′-GCAAATGATCTCCTGGGTTG-3′.

Hydrogel fabrication. We fabricated polyethylene glycol (PEG) hydrogels from PEG precursors, synthesized as described previously[32]. Briefly, we formed hydrogels by mixing 10% (wt/vol) solutions of PEG-sulfhydryl (4-arm 10-kDa PEG-SH) and PEG-vinylsulfone (8-arm 10-kDa PEG-VS) precursor polymers diluted in water or triethanolamine, respectively. We functionalized hydrogel surfaces through covalent cross-linking reaction with PBS-dialyzed laminin protein (Roche). We fabricated soft 12-kPa (Young's modulus) stiffness hydrogels to 1-mm thickness[32]. We fabricated hydrogels to a 1-μm thickness directly onto tissue culture plastic dishes to achieve a rigid 1×10^6-kPa stiffness[32], as hydrogels of ≤1-μm thickness allow cells to sense the underlying substrate mechanical properties, resulting in an effective rigidity equivalent to tissue culture plastic[32,57], while providing equivalent material surface chemistry as thicker soft gels. This nonswelling gel chemistry results in equivalent laminin protein concentrations (estimated to be 7.5 ng cm^{-2} in ref. 32) on both soft and rigid hydrogels. We fabricated hydrogel microwell arrays for clonal proliferation experiments as described previously[32]. We cut and adhered all hydrogels to cover the surface area (2.0 cm^2) of 24-well culture plates.

Muscle stem cell culture, treatment and lentiviral infection. Following isolation, we resuspened MuSCs in myogenic cell culture medium containing DMEM/F10 (50:50), 15% FBS, 2.5 ng ml^{-1} fibroblast growth factor-2 (FGF-2 also known as bFGF) and 1% penicillin-streptomycin. We seeded MuSC suspensions at a density of 1,000 cells per well (2.0 cm^2 surface area). We maintained cell cultures at 37 °C in 5% CO_2 and changed medium daily. For p38α/β inhibition studies, we added 0.05–25 μM SB202190 (EMD Chemicals) or 1 μM BIRB 796 (Axon MedChem) daily and compared these treatments with their solvent (DMSO, 0.1% final) control. We performed all MuSC cell culture assays and transplantations after 1 week of culture unless noted otherwise. For syngeneic transplant studies, we infected cultured MuSCs with elongation factor-1α promoter–driven *luc*-IRES-*GFP* lentivirus, as described below.

P16^{Ink4a} and p21^{Cip1} immunocytometric analysis. We analyzed MuSCs from young or aged mice following FACS purification or after 1 week of culture on 12-kPa hydrogels with exposure to 0.1% DMSO control or 10 μM SB202190. We collected cultured cells by incubation with 0.5% trypsin in PBS for 2 min at 37 °C. We cytopsun isolated cells to glass slides and fixed with 0.5% paraformaldehyde in PBS. We blocked fixed cells with 20% goat serum and 0.5% Triton X-100 in PBS. We stained cells with mouse monoclonal anti-p16^{Ink4a} IgG2a (Santa Cruz Biotechnology, Santa Cruz, CA, catalog # 1661, 1:100) and rabbit anti-p21^{Cip1} IgG (Abcam, Cambridge, MA, catalog # ab7960, 1:50) primary antibodies. To visualize primary antibody labeling, we stained cells with AlexaFluor 594–conjugated donkey anti-mouse IgG and AlexaFluor 488–conjugated donkey anti-rabbit IgG secondary antibodies (Jackson ImmunoResearch Laboratories, catalog # 715-585-150 and 711-545-152, respectively, 1:250 each). We counterstained nuclei with TO-PRO-3 (Invitrogen, 1:500). We acquired immunofluorescence images using a LSM510 laser-scanning confocal microscope (Carl Zeiss Microimaging) with a Plan NeoFluar 20×/0.75NA objective. We captured digital images using LSM510 software. We composed multipanel images in Photoshop software (Adobe). We reduced background and enhanced contrast equivalently across all images of the same stain.

Phosphoprotein flow cytometry. We assayed the phosphorylation of p38α/β MAPK and HSP27, readouts of p38 pathway activity, and c-Jun, a readout of c-Jun N-terminal kinase pathway activity, by phosphoprotein flow cytometry. To assay phospho-p38α/β MAPK in freshly isolated MuSCs, we dissociated hindlimb skeletal muscles and then digested them for 90 min to isolate cells. We stained these cell suspensions for MuSC sorting markers (omitting propidium iodide) and then purified them by FACS as described above. We collected the sorted cells and immediately fixed them with 1.5% paraformaldehyde in PBS and then permeabilized them in methanol at −80 °C. We then washed the cells two times with staining buffer (0.5% BSA, 2.5 mM EDTA in PBS) and blocked them in staining buffer for 30 min at room temperature. We stained cells with a mouse anti–phospho (Thr180/Tyr182)-p38α/β MAPK IgG primary antibody (Cell Signaling Technology, catalog # 9216, 1:50) and then with AlexaFluor 488–conjugated donkey anti-mouse IgG secondary antibody (Jackson ImmunoResearch Laboratories, catalog # 715-545-150, 1:250). We analyzed cells by gating again for CD45$^-$CD31$^-$CD11b$^-$Sca1$^-$CD34$^+$integrin α_7^+ MuSCs and then analyzing these cells for phospho-p38α/β MAPK positivity on a modified FACStar Plus flow cytometer using FACSDiva software (BD Biosciences).

For culture studies, we maintained MuSCs on 12-kPa hydrogels and treated them daily with either 0.1% DMSO control or 10 μM SB202190. After 7 d of culture, we collected cells by incubation with 0.5% trypsin in PBS for 2 min at 37 °C. We fixed and permeabilized cells as described above and stained them with a rabbit anti–phospho (Ser82)-HSP27 (Cell Signaling, catalog # 2401, 1:100) or a rabbit anti–phospho (Ser63)-c-Jun (Cell Signaling, catalog # 9261, 1:100) primary antibody. Then, we stained cells with AlexaFluor 488–conjugated donkey anti-rabbit secondary antibody (Jackson ImmunoResearch Laboratories, catalog # 711-545-152, 1:200). We washed cells twice with staining buffer and analyzed them on a FACSCalibur flow cytometer using the CellQuest software (both BD Biosciences).

Bulk proliferation assays. To assay bulk proliferation, we seeded MuSCs on flat hydrogels at a density of 1,000 cells per 2.0 cm^2 surface area. After 1 week, we collected cells by incubation with 0.5% trypsin in PBS for 2 min at 37 °C and counted them using a hemocytometer.

Gene expression knockdown by siRNA treatment. To knock down *Mapk14* (encoding p38α) and *Mapk11* (encoding p38β) expression, we cultured MuSCs from aged mice on collagen-coated tissue culture plastic for 1 d, collected them by incubation with 0.5% trypsin in PBS for 2 min at 37 °C and then transferred them

doi:10.1038/nm.3464

to laminin-functionalized hydrogels for 6 d. We transfected siRNA sequences (Ambion Silencer Select from Life Technologies, Carlsbad, CA) targeting p38α (*Mapk14*; ID s77114) or p38β (*Mapk11*; ID s72152) or scrambled control (100 nM; ID negative control #2) at 100 nM once on the first day of culture using siIMPORTER reagents (Upstate, Charlottesville, VA). To test the specificity of individual siRNAs (each at 100 nM), we assayed the expression of p38α (*Mapk14*) and p38β (*Mapk11*) by RT-qPCR at day 3 after treatment and compared to cells treated with the scramble control (100 nM; **Supplementary Fig. 4a**,**b**). To test the efficacy of pooled p38α/β siRNAs (100 nM each), we assayed the expression of p38α (*Mapk14*) and p38β (*Mapk11*) by RT-qPCR at day 5 after treatment and compared to cells treated with the scramble control (200 nM; **Supplementary Fig. 4c**,**d**). We also assayed phospho-HSP27, cell proliferation and myogenic gene expression in cultured MuSCs from aged mice treated with pooled 100 nM p38α/β siRNAs or 200 nM scrambled control (**Fig. 3a**–**c**,**g**,**h**).

Clonal muscle stem cell cell proliferation and fate analyses. We seeded MuSCs at a density of 500 cells per 2.0 cm^2 surface area hydrogel microwells with 600-μm diameter. This seeding density ensures that >90% of microwells contain a single cell. We monitored cell proliferation by time-lapse microscopy from 12 h (day 0) to 6 d after seeding and recorded images every 5 min at 10× magnification using a PALM/AxioObserver Z1 system (Carl Zeiss MicroImaging) with a custom environmental control chamber and motorized stage. We changed medium every other day by 'pausing' the acquisition for <5 min. At the conclusion of the experiment, we fixed cells with 2% paraformaldehyde for 10 min and blocked them with 20% goat serum and 0.5% Triton X-100 in PBS. We stained cells with a mouse monoclonal anti-myogenin antibody (BD Biosciences, catalog # 556358, 1:100) and then AlexaFluor 594–conjugated donkey anti-mouse secondary antibody (Jackson ImmunoResearch Laboratories, catalog # 715-585-150, 1:200). We counterstained nuclei with TO-PRO-3 (Invitrogen, 1:500). We acquired immunofluorescence images using a LSM510 laser-scanning confocal microscope (Carl Zeiss Microimaging) with a Plan NeoFluar 20×/0.75NA objective. We captured digital images using LSM510 software. We composed multipanel images in Photoshop software (Adobe). We reduced background and enhanced contrast equivalently across all images of the same stain. We analyzed time-lapse image sequences using the Baxter algorithm[32] in Matlab (MathWorks) to automatically identify and track single cells and generate hierarchical lineage trees.

Viable and dead cells were distinctly evident from time-lapse sequences due to phase-contrast boundary and motility maintenance or loss, respectively. We determined the clonal viability percentage (**Supplementary Fig. 3b**) by relating the number of nondividing clones that died during the long-term observation (by day 6) to the total number of viable clones observed on day 0. We determined the clonal division percentage (**Figs. 2c** and **3d**) by relating the number of clones that divided at least once by day 6 to the total number of viable clones observed on day 0. We determined the total progeny of each clone from all viable cells within the dividing clone population (**Fig. 4i**). We determined the clonal differentiation percentage (**Fig. 4i**) by relating the number of myogenin$^+$ cells to the total number of TO-PRO-3–stained cells at the culture endpoint in dividing clones.

Pax7 and myogenin expression by flow cytometry. We isolated MuSCs from aged mice by FACS sorting and cultured them on 12-kPa hydrogels with either 0.1% DMSO control or 10 μM SB202190. After 1 week of culture, we collected cells by incubation with 0.5% trypsin in PBS for 2 min at 37 °C, fixed them in 1.5% paraformaldehyde and permeabilized them in methanol at −80 °C. We then washed cells two times with staining buffer (0.5% BSA, 2.5 mM EDTA in PBS) and blocked them in staining buffer for 30 min at room temperature. We stained cells with rabbit polyclonal anti-myogenin IgG (Santa Cruz Biotechnology, catalog # sc576, 1:100) and mouse anti-Pax7 IgG1 (Santa Cruz Biotechnology, catalog # sc81648, 1:50) primary antibodies for 1 h at room temperature. Subsequently, we washed cells and incubated them with AlexaFluor 488–conjugated donkey anti-rabbit and AlexaFluor 647–conjugated donkey anti-mouse IgG1 secondary antibodies (Jackson ImmunoResearch Laboratories, catalog # 711-545-152 and 715-605-150, respectively, 1:200 each) for 30 min at room temperature. We then washed cells twice with staining buffer and analyzed them on a FACSCalibur flow cytometer using CellQuest software (both BD Biosciences). In select studies (**Fig. 3i**), we combined anti-Pax7 and anti–phospho-HSP27 immunostaining analyses.

Quantitative RT-PCR. We isolated RNA from freshly isolated and cultured cells using the RNeasy Micro Kit (Qiagen). We reverse-transcribed cDNA from total mRNA from each sample using the High Capacity cDNA RT Kit (Applied Biosystems). We subjected cDNA to RT-PCR using a SYBR Green PCR Master Mix (Applied Biosystems) in an ABI 7900HT Real-Time PCR System (Applied Biosystems). We cycled samples at 95 °C for 10 min and then 40 cycles of 95 °C for 15 s and 60 °C for 1 min. To quantify relative transcript levels, we used the $2^{-\Delta\Delta Ct}$ method to compare treated and untreated samples. *Gapdh* was used as a normalizing gene. We designed primer sequences for *Gapdh*[58], *Myog*, *Pax7* (ref. 59), *Mapk14* (p38α) and *Mapk11* (p38β) using NIH Primer3 or the cited report: *Gapdh*, forward 5′-CACTGAGCATCTCCCTCACA-3′, reverse 5′-TGGGTGCAGCGAACTTTATT-3′; *Myog*, forward 5′-TGTTTGTAAAGCTGCCGTCTGA-3′, reverse 5′-CCTGCCTGTTCCCGGTATC-3′; *Pax7*, forward 5′-CTGGATGAGGGCTCAGATGT-3′, reverse 5′-GGT TAGCTCCTGCCTGCTTA-3′; *Mapk14*, forward 5′-AAGACTCGTTGGAACCCCAG-3′, reverse 5′-GGGTCGTGGTACTGAGCAAA-3′; and *Mapk11*, forward 5′-TACCTCGTGACGACCCTGAT-3′, reverse 5′-CGGTCATCTCCTCATCAGCC-3′.

Detection of donor-derived cells within the *in vivo* satellite cell niche and their response to injury. We collected the culture progeny of MuSCs from aged *Myf5-lacZ* transgenic mice[11,45] by incubation with 0.1% trypsin in PBS for 2 min at 37 °C and transplanted them into tibialis anterior muscles of hindlimb-irradiated NOD-SCID mice. One month after transplant, we injected notexin to damage recipient muscles and activate MuSCs *in vivo*. Four days later, we collected, fixed and cryosectioned recipient muscles, as described above. We performed immunohistological analysis of transverse tissue sections to detect β-galactosidase$^+$ cells (indicating a donor-derived cell expressing Myf5, a marker of MuSC activation) in the satellite cell position within the myofiber basal lamina, as defined by laminin staining. We stained sections with anti-laminin (Millipore, clone A5, catalog # 05-206, 1:250) and anti–β-galactosidase (Invitrogen, catalog # A11132, 1:100) primary antibodies and then with AlexaFluor 594–conjugated donkey anti-rat IgG1 and AlexaFluor 488–conjugated donkey anti-rabbit (Jackson ImmunoResearch Laboratories, catalog # 712-585-150 and 711-545-152, respectively, 1:200 each) secondary antibodies. We counterstained nuclei with Hoechst 33342 (Invitrogen). We acquired images with an AxioPlan2 epifluorescent microscope (Carl Zeiss) with Plan NeoFluar 10×/0.30NA or 20×/0.75NA objectives (Carl Zeiss) and an ORCA-ER digital camera (Hamamatsu). We captured digital images in OpenLab software (Improvision) and assembled them using Photoshop software (Adobe) with consistent contrast adjustments across all images.

***GFP* transgene expression following lentiviral vector infection.** We infected cultured MuSCs with an elongation factor-1α promoter–driven *luc*-IRES-*GFP* lentivirus, generated as described previously[46,60]. We added lentivirus at 10,000 U ml^{-1} (10 multiplicity of infection) in myogenic cell culture medium (1 ml per well) supplemented with 4 μg ml^{-1} protamine sulfate from 24 to 48 h after seeding. We collected cultured cells at day 7 after seeding by incubation with 0.5% trypsin in PBS for 2 min at 37 °C. We washed cells with 20% goat serum and 0.5% Triton X-100 in PBS. We analyzed GFP expression (see **Supplementary Fig. 8a**) on a modified FACStar Plus flow cytometer using FACSDiva software (BD Biosciences).

***In vivo* force measurements.** We performed force measurements on tibialis anterior (TA) muscles *in vivo* in anesthetized mice, as previously described[46,47]. For each mouse, we shaved its hindlimbs and fixed them to a frame to immobilize it without compromising the blood supply to the leg. We warmed the mouse on an isothermal pad and by heat lamp. We made a small incision in the skin directly above the TA muscle. We sutured the distal tendon to a thin metal hook and then attached to a 300C-LR force transducer (Aurora Scientific). We cut the distal tendons from all front lower hindlimb muscles other than TA, leaving the TA isolated during attachment to the force transducer. We kept the muscles and tendons moist by periodic wetting with saline (0.9% sodium chloride) solution.

We placed a bipolar electrical stimulation cuff around the central third of the TA. In all measurements, we used 0.1-ms pulses at predetermined supramaximal stimulation intensity. For twitch force measurements, we stimulated the muscle with a single 0.1-ms pulse. For tetanic force measurements, we stimulated the muscle at 150 Hz for 0.3 s. We recorded muscle force and synchronization pulses for 2 s immediately before the stimulation and 3 s after the end of the stimulation. We performed five twitch and then five tetanic measurements on each muscle, with 3–5 min between each measurement. We collected data with a PCI-6251 acquisition card (National Instruments) and analyzed it in Matlab. We calculated specific force values by normalizing the force measurements by the muscle physiological cross-sectional area (PCSA), as described previously[61].

$$\text{PCSA} = (\text{muscle volume}/\text{fiber length}) \times (\cos\phi_{\text{fibers}})$$

ϕ_{fibers} is the pennation angle of the muscle fibers. We determined muscle volume by displacement and measured fiber length by micrometer.

Statistical analyses. We performed cell culture experiments with at least three replicates. For single-cell gene expression, proliferation and immunofluorescence assays, we report the number of individual cells quantified in the legends. We used Fisher's exact tests in comparisons between conditions for single-cell assays and transplant engraftment frequencies. For transplant studies, we performed preliminary experiments then performed power analyses of the Fisher's test before conducting our experiments in order to determine the lowest number of transplant recipients required to achieve statistical significance. In general, we performed primary transplant experiments in at least three independent experiments, with at least 15 total transplants per condition, unless otherwise noted. In some cases, we powered our studies with unbalanced numbers of replicates (see **Fig. 4b** and **Supplementary Fig. 1d**) based on these power analyses. We used unpaired two-tailed (Student's) *t*-tests to compare between conditions for bulk and clonal proliferation, gene expression, flow cytometric and force assays. We used a paired two-tailed *t*-test to compare between conditions for serial transplant assays within shared cohorts of mice. We used unpaired two-tailed Mann-Whitney *U*-tests to compare between conditions for myofiber counting and clone size and differentiation assays due to non-normality. We present box-and-whisker plots with a median central line, 50% confidence interval box and 95% confidence interval whiskers. We used a significance level of $\alpha = 0.05$ for all tests.

57. Engler, A.J., Sen, S., Sweeney, H.L. & Discher, D.E. Matrix elasticity directs stem cell lineage specification. *Cell* **126**, 677–689 (2006).
58. Pajcini, K.V., Corbel, S.Y., Sage, J., Pomerantz, J.H. & Blau, H.M. Transient inactivation of Rb and ARF yields regenerative cells from postmitotic mammalian muscle. *Cell Stem Cell* **7**, 198–213 (2010).
59. Le Grand, F., Jones, A.E., Seale, V., Scime, A. & Rudnicki, M.A. Wnt7a activates the planar cell polarity pathway to drive the symmetric expansion of satellite stem cells. *Cell Stem Cell* **4**, 535–547 (2009).
60. Westerman, K.A., Ao, Z.J., Cohen, E.A. & Leboulch, P. Design of a trans protease lentiviral packaging system that produces high titer virus. *Retrovirology* **4**, 96 (2007).
61. Sacks, R.D. & Roy, R.R. Architecture of the hindlimb muscles of cats: functional significance. *J. Morphol.* **173**, 185–195 (1982).

doi:10.1038/nm.3464